PAPER

CrossMark
← click for updates

Synthesis of nitrogen-doped ZnO by sol–gel method: characterization and its application on visible photocatalytic degradation of 2,4-D and picloram herbicides†

J. J. Macías-Sánchez,[a] L. Hinojosa-Reyes,[a] A. Caballero-Quintero,[b] W. de la Cruz,[c] E. Ruiz-Ruiz,[a] A. Hernández-Ramírez[a] and J. L. Guzmán-Mar*[a]

In this work, nitrogen-doped ZnO material was synthesized by the sol–gel method using zinc acetate as the precursor and urea as the nitrogen source (15, 20, 25 and 30% wt.). For comparative purposes, bare ZnO was also prepared. The influence of N doping on structural, morphological, optical and photocatalytic properties was investigated. The synthesized catalysts were characterized by XRD, SEM-EDS, diffuse reflectance UV-Vis spectroscopy, BET and XPS analysis. The photocatalytic activity of N-doped ZnO catalysts was evaluated during the degradation of a mixture of herbicides (2,4-D and picloram) under visible radiation ≥400 nm. The photo-absorption wavelength range of the N-doped ZnO samples was shifted to longer wavelength compared to those of the unmodified ZnO. Among different amounts of dopant agent, the 30% N-doped ZnO material showed higher visible-light activity compared with pure ZnO. Several degradation by-products were identified by using HPLC and ESI-MS/MS. The enhancement of visible photocatalytic activity of the N-doped ZnO semiconductor could be mainly due to their capability in reducing the electron–hole pair recombination.

Introduction

Zinc oxide (ZnO) is a widely used photocatalyst owing to its high activity and low cost, and has attracted much attention in the field of environmental research, where it is commonly used for the degradation of various recalcitrant organic pollutants such as herbicides in aqueous solution.[1]

However, the photocatalytic activity of ZnO is limited to UV irradiation because it is a semiconductor with a wide band-gap of about 3.2 eV and can only absorb UV light with $\lambda \leq$ 387 nm.[2] Therefore visible light responsive catalysts are highly desired due to the low cost of energy involved and the possibility of using solar energy to activate the photocatalyst.

[a]Universidad Autónoma de Nuevo León, UANL, Facultad de Ciencias Químicas, Cd. Universitaria, San Nicolás de los Garza, Nuevo León C.P. 66451, Mexico. E-mail: jorge.guzmanmr@uanl.edu.mx
[b]Procuraduría General de Justicia del Estado de Nuevo León, Laboratorio de Química Forense, Criminalística y Servicios Periciales, Av. Gonzalitos 452, Col. Residencial Galerías, Monterrey, NL C.P. 66451, Mexico
[c]Universidad Nacional Autónoma de México, UNAM, Centro de Nanociencias y Nanotecnología, Km 107 Carretera Tijuana-Ensenada, C.P. 22800 Baja California, Mexico
†This paper is published as part of the themed issue of contributions from the 8th European Meeting on Solar Chemistry and Photocatalysis: Environmental Applications held in Thessaloniki, Greece, June 2014.

Additionally, some problems still remain to be solved in the application of ZnO semiconductors, such as the fast recombination of photogenerated electron–hole pairs.[3] For that reason is important to evaluate new modified ZnO catalysts with improved photocatalytic activity and enhanced activities under both UV and visible light irradiation.[2–5]

Recent investigations to activate ZnO have been focused on doping ZnO with transition metals such as manganese, ruthenium and vanadium using sol–gel or co-precipitation methods.[4,6,7] However, the thermal instability and the increase of carrier recombination centers greatly limit the performance of transition metal dopants.[8] One way to avoid this limitation is to dope non-metals such as nitrogen, sulphur, and carbon into the substitutional sites in the crystal structure of the photocatalyst.[9–12]

Therefore, the anionic non-metal impurities are presented as better options for incorporation as dopants into the substitutional sites in the crystal structure of a photocatalyst because of their closer position to the oxygen in the periodic table.[9]

The incorporation of this type of dopant in the crystal structure of the semiconductor promotes narrowing of the band gap, causing its activation with lower energy radiation.[13] Nitrogen-doped ZnO catalyst (N-ZnO) has been synthesized by thermal decomposition of zinc nitrate at 350 °C. This material showed improvement over undoped ZnO in its optical

absorption and photocatalytic activity on the reduction of Cr(VI) and the oxidation of methyl orange under visible light radiation.[14] Thin films of N-ZnO were also synthesized *via* spray pyrolysis technique in aqueous medium using zinc acetate and ammonium acetate as precursors. The rate of degradation of toluene over N-doped ZnO was higher as compared to that of pure ZnO under solar illumination.[12]

In this work, the synthesis of N-ZnO photocatalyst by the sol–gel method was proposed since this method allows the incorporation of the dopant into the crystal lattice of the material[15] using urea as nitrogen precursor. Among the nitrogen sources, urea is an inexpensive reagent that has demonstrated to lead to controlled nucleation and growth of nanocrystals, allowing the formation of well-ordered mesoporous structures.[16] To the best of our knowledge, the successful incorporation of nitrogen in TiO$_2$ using the sol–gel process has already been demonstrated,[17–19] but there are no reports in synthesizing N-ZnO photocatalyst by the sol–gel method. In the sol–gel process, the doping levels as well as the size of nanoparticles can be easily controlled depending on the reaction conditions such as the solvents used, pH, temperature, and hydrolysis rate.[15] Moreover, the utilization of N-ZnO photocatalyst in degrading 2,4-dichlorophenoxyacetic acid (2,4-D) and 4-amino-3,5,6-trichloro-2-pyridinecarboxylic acid (picloram) mixture in aqueous solution under visible radiation has not been reported so far. 2,4-D is extensively used worldwide due to its low cost for selective weed control in gardens and farmlands. It has led to its frequent detection in groundwater.[3,20] Picloram is a potent herbicide that effectively controls the growth of broadleaf weed and woody plants in pastures and rangelands. Picloram is poorly bound to soil and its water solubility (440 mg L^{-1}) makes it a potentially mobile compound. These properties, combined with being relatively persistence in soil, mean that the use of picloram can cause groundwater contamination.[13,21] Commercial formulations usually available in Mexico contain these herbicides in mixture *e.g.* Tordon 101, Tordon 472, *etc.* Therefore, the photocatalytic degradation of a 2,4-D and picloram mixture was undertaken under visible radiation using N-ZnO catalyst. An attempt was also made to identify the intermediate products formed during the photocatalytic process through HPLC and ESI-MS/MS analysis.

Experimental section

Chemicals

Zinc acetate (99.6% purity) was purchased from J. T. Baker. Ammonium hydroxide (50% v/v) reagent grade was from Reactivos Monterrey. Urea (99% purity), acetonitrile (HPLC grade), sodium hydroxide (97% purity) and phosphoric acid (85%, v/v) were from Sigma-Aldrich. 2,4-D (98% purity) and picloram (99.6%) analytical grade herbicides were obtained from Spectrum and Fluka, respectively. Stock solutions of the herbicides (100 mg L^{-1}) were prepared in volumetric glassware. The required working standards were prepared daily from the stock

solutions. All other reagents were reagent grade and used as received. All solutions were prepared with ultrapure water (18 MΩ cm^{-1}) from a Millipore Milli-Q system.

Synthesis of ZnO and N-ZnO

N-ZnO material was prepared by the sol–gel method using zinc acetate as the precursor and urea as the nitrogen source; the [N]/[Zn] ratios of the doped materials calculated on the basis of the weight percent used in the starting solution were 15, 20, 25 and 30%. The technique is briefly described as follows: 13.5 g of zinc acetate and urea was dissolved in 250 mL of water. An aqueous solution (50% v/v) of NH$_4$OH was added under continuous magnetic stirring to reach a pH of 8.5. The reaction mixture was kept at room temperature until the gelation was started. The obtained gel was aged for 24 h at room temperature to complete the polymerization, filtered, washed with 0.1 M NH$_4$NO$_3$, and subsequently dried by heating slowly to 90 °C until the solvent was completely evaporated. The resulting powder was calcined at 400 °C for 5 h in air with heating rate of 10 °C min^{-1}. The pure ZnO catalyst was prepared by the same procedure without addition of urea.

Catalyst characterization

The structural properties of the catalysts were studied by X-ray diffraction (XRD) (Siemens D5000) using Cu Kα radiation (λ = 1.5418 Å). BET surface areas were calculated from N$_2$ adsorption–desorption isotherms obtained on an Autosorb-1 instrument (Quantachrome Co., Boynton Beach, FL, USA). The band gap energy (E_g) values of the studied catalysts were calculated from the UV-Vis diffuse reflectance spectra using a Thermo Scientific Evolution 300 UV-Vis spectrophotometer (Thermo Fisher Scientific, Massachusetts, USA) equipped with an integrating sphere TFS-Praying Mantis. Spectralon sample was used as the reference. The morphology of the catalysts was examined using JEOL JSM-6701F scanning electron microscopy (SEM) and energy dispersive spectroscopy (EDS) on powder samples directly sprinkled over aluminium foil under high vacuum and accelerating voltage of 12 kV. X-ray photoelectron spectroscopy (XPS) analyses were performed on a multi-technique system (SPECS) equipped with a dual Mg/Al X-ray source and hemispherical PHOIBOS 150 WAL analyzer operating in the fixed analyzer transmission (FAT) mode. The spectra were obtained at 1486.74 eV using Al Kα as the X-ray source. The anode was operated at a voltage of 14.5 kV and source power level was set to 350 W. The binding energies were referenced to the carbon (C1s) peak at 285.0 eV to compensate for charging effects and the peak positions were compared to standard values for identification of different elements and their oxidation states.

Evaluation of the photocatalytic activity

The photocatalytic experiments were performed in a Pyrex reaction vessel (200 mL capacity) containing an aqueous solution of a mixture of 20 mg L^{-1} 2,4-D and 5 mg L^{-1} picloram. The solution pH was adjusted to 7 by the addition of 0.1 M NH$_4$OH. As radiation source, a visible 25 W tungsten–halogen

(Philips Electronics, 760 W m^{-2}) lamp was used, which emits polychromatic radiation in the spectral range from 400 to 700 nm (with the maximum in the wavelength range 540–620 nm).

The on-line monitoring of the concentration of each herbicide was performed using an automated multisyringe chromatographic system (MSC).[22] The MSC equipment consisted of a multisyringe module (BU-4 S, Crison; Alella, Barcelona, Spain) with four 5 mL syringes (S1–S4) (Hamilton, Bonaduz, Switzerland) and an 8-port multi-position selection valve (MPV, Crison Instruments, Alella, Spain), each of which was connected at the head to a three-way solenoid valve (N-Research, Caldway, NJ, USA).

The detection system consisted of a DT-1000CE deuterium light source (Analytical Instrument System, Flemington, NJ, USA) and a USB2000 CCD spectrophotometer (Ocean Optics, Dunedin, FL, USA) connected to a flow-through quartz cell (178.711-QS; Hellma, NY, USA). Measurements were recorded at 250 nm. Autoanalysis v5.0 software (Sciware, Palma de Mallorca, Spain) was used for instrument control, data acquisition, and data processing. Quantitative analysis was based on peak height. Chromatographic separation of 2,4-D and picloram was performed on an Onyx™ C18 monolithic column (25 × 4.6 mm, Phenomenex) with a 10 × 4.6 mm monolithic guard column. The manifold was built from 0.8 and 1.5 mm i.d. Teflon tubing. The mobile phase used for chromatographic separation was 5 mM H_3PO_4–acetonitrile (70 : 30, v/v) with a flow rate of 1 mL min^{-1}. The photocatalytic reactions were conducted in triplicate.

The mineralization percentage was assessed by determining the total organic carbon (TOC) content in the aqueous solution with a TOC-V CSH Shimadzu Analyzer.

Generated carboxylic acids were detected by ion-exclusion chromatography using a Bio-Rad Aminex HPX-87H column (300 × 7.8 mm) with UV detection (210 nm) using 14 mM H_3PO_4 mobile phase at 0.4 mL min^{-1}.

The by-products from the photocatalytic degradation were identified by an ESI-MS/MS mass spectrometer AB Sciex API 4000 operating in the negative ion mode. The reaction aliquots were directly infused into the ion source at a flow rate of 20 μL min^{-1} using a micro syringe (Hamilton Company, Reno, NV, USA) and the related mass spectra obtained as an average of 1463 scans, each one requiring 0.2 s. Typical ESI conditions were as follows: heated capillary temperature, 200 °C; sheath gas (N_2) at a flow rate of 20 mL min^{-1}; spray voltage, −5.5 kV; nebulizing gas, and curtain gas flows were at instrument settings of 30, and 10 mL min^{-1}, respectively.

Results and discussion

Characterization

The diffraction patterns of ZnO and N-doped ZnO (15, 20, 25 and 30%) semiconductors are shown in Fig. 1.

It can be seen that N-containing ZnO powder exhibits dominant diffraction peaks of wurtzite phase (JCPDS: 36-1451) with
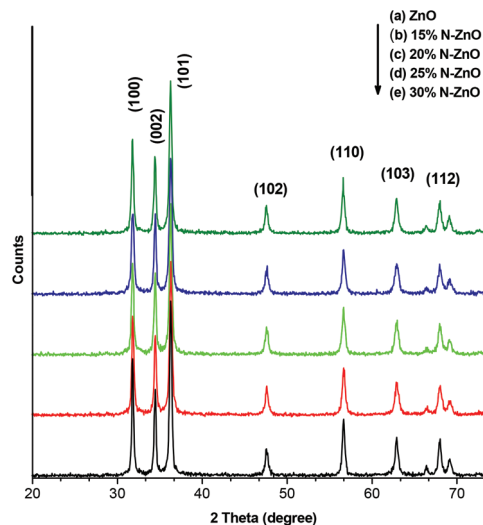
Fig. 1 XRD patterns of ZnO and N-doped ZnO catalysts prepared by sol–gel method.

Table 1 Specific surface area, crystallite size and E_g values for N-doped ZnO and pure ZnO

Sample	BET area ($m^2\ g^{-1}$)	Crystallite size (nm)	E_g value (eV)
ZnO	18.50	36.20	3.06
15% N-ZnO	13.77	31.13	2.97
20% N-ZnO	18.72	28.54	2.85
25% N-ZnO	25.80	27.63	2.90
30% N-ZnO	21.95	28.84	2.87

good crystallinity. The introduction of nitrogen atoms did not change the ZnO crystal structure. Crystallite sizes of the N-containing ZnO were calculated from the X-ray peak broadening of the (101) diffraction peak using the Scherrer formula.[23] The crystallite sizes of N-containing ZnO are shown in Table 1 along with other physical characteristics. It can be seen from Table 1 that the crystallite size of N-ZnO materials decreased with the increase of nitrogen present in the material, up to 25%. This result was consistent with those reported by Qin et al.,[11] who indicated that during preparation of N-doped ZnO catalysts, the addition of urea, which behaves as a surfactant, could inhibit the growth of ZnO.

BET surface areas are also given in Table 1. The specific surface area varied from 18.50 to 25.80 m^2 g^{-1}, and its maximum value was observed on 25% N-doped ZnO. This value is higher than the value of 18.95 m^2 g^{-1} for pure ZnO, indicating that the introduction of nitrogen facilitated the formation of particles with porous surfaces. Optical characterization was performed by measuring the UV-Vis diffuse reflectance spectrum to determine the E_g value of each material using the Kubelka–Munk function $F(R)$ (1).[24]

$$F(R) = (1 - R)/2R \qquad (1)$$

where R is the magnitude of reflectance and $F(R)$ is proportional to the extinction coefficient (α). The Kubelka–Munk
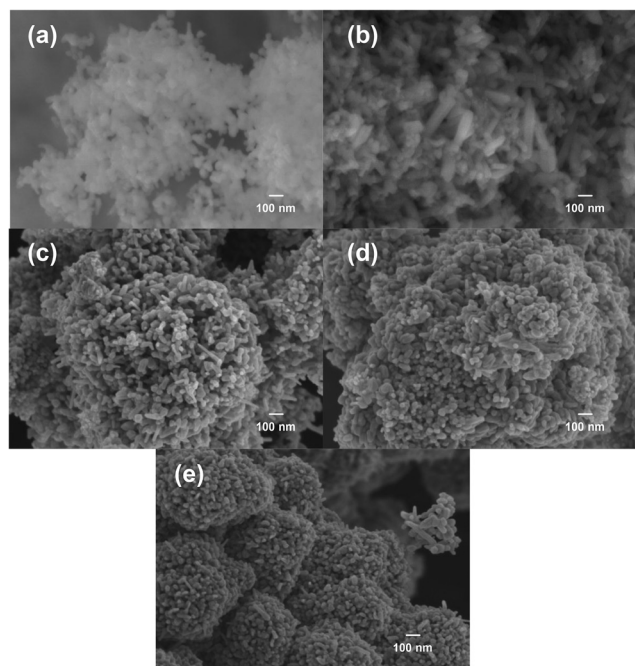
Fig. 2 SEM images at 50 000× magnification of (a) ZnO, (b) 15% N-ZnO, (c) 20% N-ZnO, (d) 25% N-ZnO and (e) 30% N-ZnO.

Fig. 3 XPS spectra of the (a) N_{1s}, (b) $Zn_{2p_{3/2}}$ and (c) O_{1s} core levels of the 30% N-ZnO catalyst. For (b) and (c) the ZnO spectrum is also shown as a reference.

function can be obtained by multiplying the $F(R)$ function by $h\nu$ using the corresponding coefficient (n) associated with an electronic transition as follows: $(F(R) \times h\nu)^{n}$; for ZnO, the value for the direct allowed sample transition is $n = 1/2$.[24,25]

As can be seen in Table 1, the E_g values of the catalysts were noted to shift to lower energies with increasing the nitrogen content in the catalyst. The increased amount of visible light energy absorbed can be related to two phenomena: introduction of surface structural defects and lattice alteration during the modification procedure. In fact, the E_g value decreased by 0.19 eV for the 30% N-doped sample compared to its value for the ZnO catalyst.

The catalysts were also analysed by SEM-EDS. Although the elemental analysis detected the presence of Zn, C and O (data no shown), changes in the morphology of the catalysts were noticed when the concentration of nitrogen increased from 15 to 30%. The N-ZnO photocatalysts consisted of agglomerates of primary particles with uniform rod-like shape of approximately 80–100 nm (Fig. 2).

The presence of nitrogen in the crystalline lattice of N-ZnO and its concentration was further confirmed by XPS. From the high resolution scanning XPS spectra of N_{1s}, a characteristic asymmetric broad peak from 398 to 402 eV with maximum at 398.5 eV related to N_{1s}[11,14] was observed in the N-ZnO material, which suggests that more than one chemical state of N is present;[26] although the peak in the XPS survey profile was weak, the peak position and its broadening were clear in the N_{1s} scan profile (Fig. 3a). Chen *et al.* reported a binding energy of 398.8 eV for the nitrogen substitution on the oxygen sublattice (NO).[14] The peak of 399.6 eV is a typical value of the N_{1s} binding energy in amines;[26] thus is reasonable to expect the
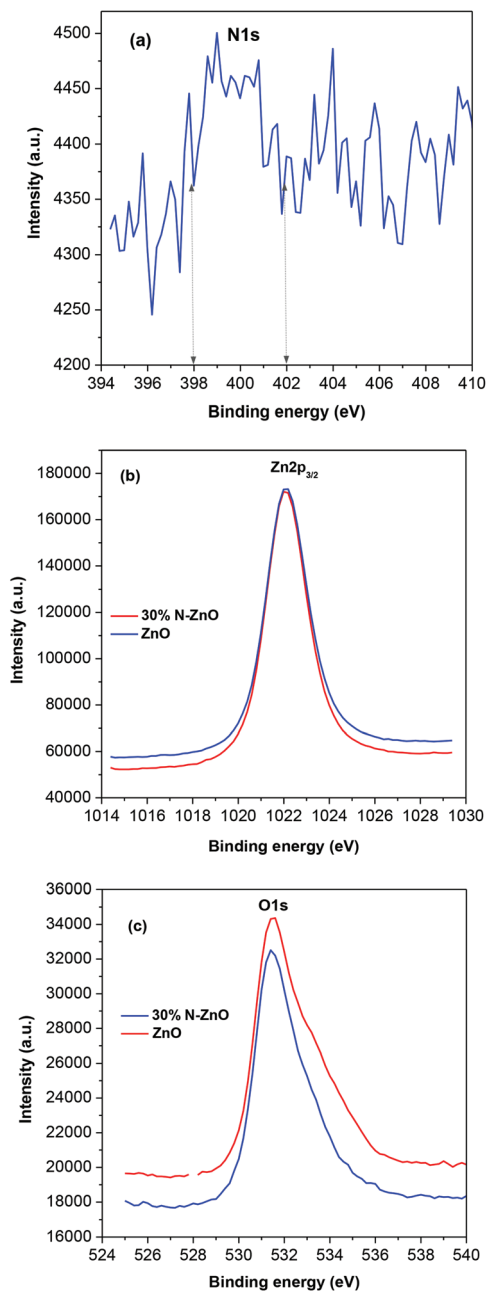
presence of N–H compounds in the N-ZnO catalyst. From the peak intensity and using the photo-ionization constants for each element (Zn, O and N), the N percentage present in the sample was calculated. The N percentage for 30% N-doped ZnO was 0.9%. This value is similar to the obtained by Chen *et al.*[14] through high resolution scanning XPS analysis, which reported an amount of 1.0 at% for a low intensity spectra. XPS is a surface chemical analysis technique that detects the elemental composition of the surface of materials (usually the top 1–10 nm).

High resolution XPS spectra of the $Zn_{2p_{3/2}}$ and O_{1s} core lines are shown in Fig. 3b and c, respectively. The core line of $Zn_{2p_{3/2}}$

for pure ZnO was located at 1021.8 eV (Fig. 3b). The asymmetric $Zn_{2p_{3/2}}$ peak for nitrogen doped ZnO was located at 1022 eV and showed superposition of Zn–O and Zn–N bonds, revealing incorporation of N in the ZnO catalyst.[27] In Fig. 3c the high resolution scanning XPS spectrum of O_{1s} after deconvolution shows that oxygen exists at least in three forms with the following binding energies: 530.5, 532.0, 533.5 eV. The peak at 530.5 eV is mainly assigned to the oxygen atoms coordinated with Zn atoms. The peak at 532 eV corresponds to oxygen adsorbed on sample surface, probably as (–OH). The peak at 533.5 eV is likely to be due to water molecules on the surface[14,28]

Photocatalytic evaluation

The photocatalytic activities of the N-ZnO materials were compared to that of ZnO sol–gel under visible irradiation for the degradation of a mixture of 20 mg L^{-1} 2,4-D and 5 mg L^{-1} picloram at pH 7 in aqueous solution using 1 g L^{-1} of catalyst. The initial concentration of the substrates was taken on basis of the concentration ratio of these herbicides in commercial formulations, where the compounds are available as mixture. An experimental design full factorial 3^2 was preliminary applied to evaluate the effect of the catalyst amount added (0.5, 1.0 and 1.5 g L^{-1}) and solution pH (5, 7 and 9). Although the pH and the catalyst amount were not dominant factors affecting the degradation rate of the pesticide mixture, it was found that the highest degradation of both compounds was observed at pH between 7.0 and 8.5 using 1 g L^{-1} of catalyst amount. The photocatalytic degradation of 2,4-D and picloram over the N-doped ZnO materials is shown in Fig. 4. As can be seen in the figure, the photocatalytic activity of 30% N-doped ZnO powder was slightly higher than that of the pure ZnO. The 30% N-doped ZnO reached 100% degradation for 2,4-D and picloram in 210 and 240 min, respectively. The results showed that the efficiency of the photocatalytic degradation is influenced by the molecular structure of the pollutant. The herbicide 2,4-D was more susceptible to hydroxyl radical attack. Conversely, the picloram oxidation reaction was slower due to greater stability of the picloram molecule conferred by the covalently bound chlorine atoms.

The photocatalytic degradation rate of pesticide compounds can be explained by a Langmuir–Hinshelwood (LH) pseudo-first-order kinetics model[1,3,21,25] with the following eqn (2):

$$\ln(C_0/C) = k_{obs}t \qquad (2)$$

where C_0 is the equilibrium concentration of herbicides (mg L^{-1}) after 1 h in dark adsorption, C is the concentration of the herbicides remaining in the solution at irradiation time t (min), and k_{obs} is the observed rate constant (min^{-1}). The summary of the pseudo-first-order kinetic values of the prepared ZnO catalysts under visible-light irradiation is shown in Table 2. The rate of degradation increases gradually with the doped level of N. The maximum k_{obs} value for 2,4-D and picloram were found during the photocatalytic degradation using 30% N-ZnO. As is clearly evident from this data the N-ZnO was more active under visible-light compared with pure
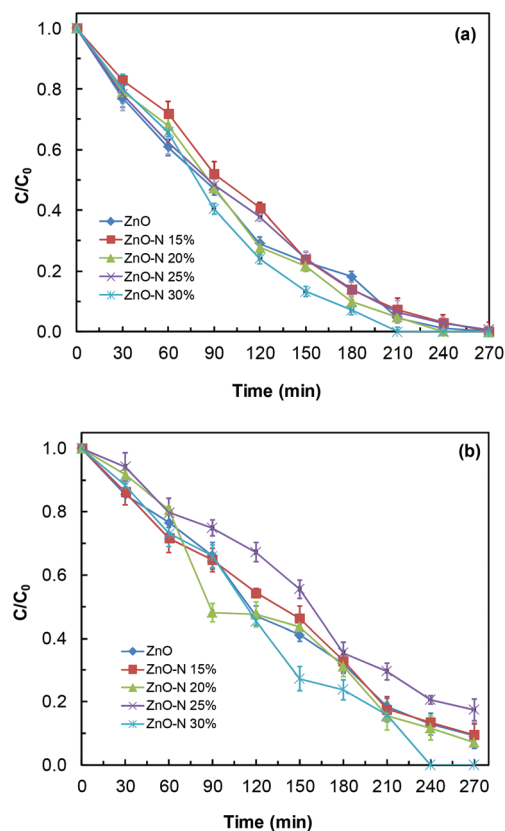
Fig. 4 Photocatalytic degradation of (a) 2,4-D (20 mg L^{-1}) and (b) picloram (5 mg L^{-1}) mixture at pH 7 and 1 g L^{-1} catalyst mass under visible radiation with N-doped ZnO catalysts with different N loadings.

ZnO. Consequently, higher mineralization was obtained in the presence of 30% N-doped ZnO after 270 min of reaction: 57% mineralization of the herbicide mixture vs. 0.2% TOC abatement with the ZnO material (Table 2). The high degradation and mineralization efficiency under visible light radiation ($\lambda > 400$ nm) of the N-doped ZnO can be explained by the presence of nitrogen species. Additionally, the N-ZnO material showed smaller crystallite size and larger surface area compared with pure ZnO, which could improve the photoactivity. The suppression of electron–hole recombination and generation of more hydroxyl radicals in the N-doped samples could play an important role in the enhanced rate of degradation under visible radiation.[12]

Table 2 Rate constant (k_{obs}) and mineralization percentage values for the photocatalytic degradation of 2,4-D and picloram mixture under visible light irradiation using N-doped catalysts

Catalyst	2,4-D		Picloram		TOC abatement (%)
	$k_{obs} \times 10^{-3}$ (min^{-1})	R	$k_{obs} \times 10^{-3}$ (min^{-1})	R	
ZnO	10.7	0.9726	7.5	0.9735	0.2
15% N-ZnO	9.8	0.9953	7.3	0.9535	29
20% N-ZnO	12.4	0.9761	8.1	0.9544	27
25% N-ZnO	10.4	0.9831	5.8	0.9588	36
30% N-ZnO	15.0	0.9820	9.1	0.9798	57
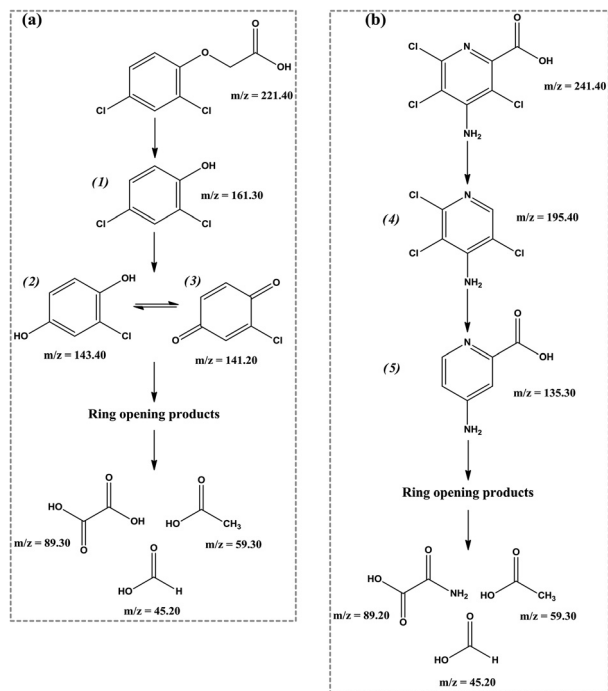
Fig. 5 Proposed fragmentation pathways of (a) 2,4-D and (b) picloram in the presence of 30% N-doped ZnO catalyst under visible radiation.

The formation of organic intermediates during the photocatalytic treatment of 2,4-D and picloram using 30% N-doped ZnO material was monitored by ESI-MS/MS. During this determination each herbicide was treated individually. Based on the information provided by the MS (the m/z values of the ionic species) and MS/MS data (the fragmentation profiles of the mass-selected ions), the proposed chemical structures of reaction products are indicated in Fig. 5. The identified intermediates during the degradation of 2,4-D were 2,4-dichlorophenol (1), which is subsequently degraded to form 2-chloro-1,4-benzoquinone (2) and chlorohydroquinone (3). Likewise, these compounds were also suggested during the degradation by oxalate-mediated photooxidation[29] and advanced electrochemical oxidation processes.[30] On the other hand, ESI-MS/MS analysis of the irradiated aqueous solution of picloram showed the formation of two main products: 4-amino-2,3,5-trichloropyridine (4) and 4-aminopyridine-2-carboxylic acid (5). The intermediate (4) was reported during the photocatalytic degradation by TiO_2 [13,21] and in the electro-Fenton process.[31] Ghauch reported the formation of (5) using zerovalent iron powder.[32] The further oxidation of the intermediate products generated short chain carboxylic acids like oxalic, oxamic, acetic and formic identified by ion-exclusion chromatography. Those compounds are recognized as much recalcitrant to oxidation.[33]

Conclusions

The nitrogen-doped ZnO semiconductors prepared by sol–gel method produced particles with nanometric size (28.84 nm).

XPS measurements demonstrated the presence of nitrogen in the N-doped ZnO material. The photocatalytic performance of modified N-ZnO nanoparticles under visible light irradiation was demonstrated by the oxidation of picloram and 2,4-D. Among different amounts of dopant agent, the 30% N-ZnO photocatalyst indicated the highest degradation efficiency due to its lower band gap energy and higher surface area. The identified by-products were transformed by ˙OH radicals into carboxylic acids such as oxalic, oxamic, acetic and formic acid. Conclusively, ZnO nanoparticles doped with 30% nitrogen can be an efficient photocatalyst for the removal of organic herbicides under visible light irradiation due to its capability for reducing electron–hole pair recombination.

Acknowledgements

Notes and references

1 S. Ahmed, M. G. Rasul, R. Brown and M. A. Hashib, *J. Environ. Manage.*, 2011, **92**, 311–330.
2 S. Rehman, R. Ullah, A. M. Butt and N. D. Gohar, *J. Hazard. Mater.*, 2009, **170**, 560–569.
3 S.-M. Lam, J.-C. Sin, A. Z. Abdullah and A. R. Mohamed, *J. Mol. Catal. A: Chem.*, 2013, **370**, 123–131.
4 J. Z. Bloh, R. Dillert and D. W. Bahnemann, *Environ. Sci. Pollut. Res. Int.*, 2012, **19**, 3688–3695.
5 D. Li and H. Haneda, *J. Photochem. Photobiol., A*, 2003, **155**, 171–178.
6 K. Rekha, M. Nirmala, M. G. Nair and A. Anukaliani, *Physica B*, 2010, **405**, 3180–3185.
7 R. Slama, F. Ghribi, A. Houas, C. Barthou and L. El Mir, *Thin Solid Films*, 2011, **519**, 5792–5795.
8 T. Umebayashi, T. Yamaki, S. Yamamoto, A. Miyashita, S. Tanaka, T. Sumita and K. Asai, *J. Appl. Phys.*, 2003, **93**, 5156–5160.
9 L.-C. Chen, Y.-J. Tu, Y.-S. Wang, R.-S. Kan and C.-M. Huang, *J. Photochem. Photobiol., A*, 2008, **199**, 170–178.
10 S. Cho, J.-W. Jang, J. S. Lee and K.-H. Lee, *CrystEngComm*, 2010, **12**, 3929.
11 H. Qin, W. Li, Y. Xia and T. He, *ACS Appl. Mater. Interfaces*, 2011, **3**, 3152–3156.
12 S. S. Shinde, C. H. Bhosale and K. Y. Rajpure, *J. Photochem. Photobiol., B*, 2012, **113**, 70–77.
13 B. Abramović, D. Šojić, V. Despotović, D. Vione, M. Pazzi and J. Csanádi, *Appl. Catal., B*, 2011, **105**, 191–198.
14 S. Chen, W. Zhao, S. Zhang and W. Liu, *Chem. Eng. J.*, 2009, **148**, 263–269.

15 M. Răileanu, M. Crișan, I. Nițoi, A. Ianculescu, P. Oancea, D. Crișan and L. Todan, *Water, Air, Soil Pollut.*, 2013, **224**, 1–45.

16 K. M. Parida and B. Naik, *J. Colloid Interface Sci.*, 2009, **333**, 269–276.

17 V. Caratto, L. Setti, S. Campodonico, M. M. Carnasciali, R. Botter and M. Ferretti, *J. Sol-Gel Sci. Technol.*, 2012, **63**, 16–22.

18 T. C. Jagadale, S. P. Takale, R. S. Sonawane, H. M. Joshi, S. I. Patil, B. B. Kale and S. B. Ogale, *J. Phys. Chem. C*, 2008, **112**, 14595–14602.

19 K. Elghniji, M. Ksibi and E. Elaloui, *J. Ind. Eng. Chem.*, 2012, **18**, 178–182.

20 L. K. Mun, A. H. Abdullah, M. Z. Hussein and Z. Zainal, *Sains Malays.*, 2014, **43**, 437–441.

21 M. Atiqur Rahman and M. Muneer, *J. Environ. Sci. Health, Part B*, 2005, **40**, 247–267.

22 C. Chávez-Moreno, J. Guzmán-Mar, L. Hinojosa-Reyes, A. Hernández-Ramírez, L. Ferrer and V. Cerdà, *Anal. Bioanal. Chem.*, 2012, **403**, 2705–2714.

23 R. Jenkins and R. Snyder, *Introduction to X-ray powder diffractometry*, John Wiley & Sons, 2012.

24 R. López and R. Gómez, *J. Sol-Gel Sci. Technol.*, 2011, **61**, 1–7.

25 M. L. Maya-Trevino, J. L. Guzman-Mar, L. Hinojosa-Reyes, N. A. Ramos-Delgado, M. I. Maldonado and A. Hernandez-Ramirez, *Ceram. Int.*, 2014, **40**, 8701–8708.

26 X. Yang, A. Wolcott, G. Wang, A. Sobo, R. C. Fitzmorris, F. Qian, J. Z. Zhang and Y. Li, *Nano Lett.*, 2009, **9**, 2331–2336.

27 L. Wang, B. Lin, L. Zhou, Y. X. Shang, G. N. Panin and D. Fu, *Mater. Lett.*, 2012, **85**, 171–174.

28 A. P. Bhirud, S. D. Sathaye, R. P. Waichal, L. K. Nikam and B. B. Kale, *Green Chem.*, 2012, **14**, 2790.

29 C. Y. Kwan and W. Chu, *Water Res.*, 2004, **38**, 4213–4221.

30 E. Brillas, J. C. Calpe and J. Casado, *Water Res.*, 2000, **34**, 2253–2262.

31 A. Ozcan, Y. Sahin, A. S. Koparal and M. A. Oturan, *J. Hazard. Mater.*, 2008, **153**, 718–727.

32 A. Ghauch, *Chemosphere*, 2001, **43**, 1109–1117.

33 B. Boye, E. Brillas, B. Marselli, P.-A. Michaud, C. Comninellis and M. M. Dieng, *Bull. Chem. Soc. Ethiop.*, 2004, **18**, 205–214.